MATERIALS CHEMISTRY
FRONTIERS

RESEARCH ARTICLE

View Article Online
View Journal | View Issue

Cite this: *Mater. Chem. Front.*, 2019, **3**, 916

Supramolecular nanocatalyst in water: successive click-driven assembly of click-derived rod amphiphiles†

Inhye Kim [ab] and Eunji Lee [*a]

Received 30th January 2019,
Accepted 25th March 2019

DOI: 10.1039/c9qm00059c

rsc.li/frontiers-materials

A supramolecular vesicular nanocatalyst (**VC**) for successive Cu^{I}-catalyzed azide–alkyne cycloaddition in water was developed by self-assembly of a click chemistry-derived rod amphiphile (**CA**). The **CA** generated by click reaction of azide-terminated benzyl ether dendrons and diethynyl naphthalene self-assembles into vesicles in water. The excellent catalytic activity of the **VC** was endowed by Cu^{I}-chelation to triazole-containing rod block within **VC** wall. The **VC** performed click reaction of benzyl azide with phenylacetylene or trimethylsilylacetylene. The resultant hydrophobic products self-encapsulated in **VC** wall affect the interfacial curvature of the **VC** according to their structural compatibility with **CA**, inducing the increase in vesicular size or structural change to micelle. Interestingly, the morphology of **VC**-derived nanocatalyst was further controlled from micelle to vesicle and *vice versa* by successive click reactions, leading to controllable loading/release of hydrophilic payloads. This recyclable catalytic activity of the self-transformable nanocatalyst was confirmed by a visually detectable click reaction offering a fluorescent color change of the aqueous **VC** solution.

Introduction

Supramolecular nanovesicles based on the aqueous self-assembly of amphiphiles possess two types of confined spaces: the aqueous core cavity and the hydrophobic wall.[1–3] The confined wall enables the vesicle to serve as a nanoreactor by providing a hydrophobic environment, where chemical reactions such as a Diels–Alder reaction,[4] palladium-catalyzed carbon–carbon bond forming reaction,[5,6] and enzymatic cascade reaction[7–9] can be performed. This ability can be used to increase the conversion efficiency by locally concentrating the reacting species and pre-organizing them in a favored conformation for a desired reaction.[10] The vesicles can also show a nanostructural change in response to external stimuli such as pH, light, temperature, and guest molecules,[11–13] resulting from the interfacial curvature change of vesicles by the dynamic assembly behavior of stimuli-responsive block-containing amphiphiles.[14,15] This makes them attractive candidates for developing transformable nanomaterials in smart chemo/biosensors and controlled drug/imaging agent delivery.[14–17] However, self-transformable nanoreactors that can act as an on-demand nanotransporter of payloads has rarely been reported.

Cu^{I}-catalyzed azide–alkyne cycloaddition (CuAAC) click chemistry, resulting in 1,4-disubstituted 1,2,3-triazole derivatives,[18–20] has led to a wealth of applications due to its synthetic simplicity, mild reaction conditions, and biocompatibility.[21–24] However, the instability of catalytically active Cu^{I} sites requires a large amount of Cu^{I} catalyst to accelerate the CuAAC click reaction. The complete removal of Cu^{I} is also a challenge and limits the utilization of click chemistry in electronics, biomedicine, and green chemistry.[25] Interestingly, the click-derived triazole group has also been attractive as a ligand providing several donor sites for chelating metal ions,[26,27] increasing its use in click chemistry with applications such as chemosensing,[28] catalysis,[29] and therapeutics.[30,31] Therefore, one can envision that the click reaction-derived rod amphiphiles spontaneously form vesicles in water, providing a hydrophobic space where catalytic Cu^{I} is chelated by a triazole group and can act as a vesicular nanocatalyst (**VC**) for click reactions.

Herein, we report the supramolecular self-transformable **VC** based on the self-assembly of a click-derived, Cu^{I}-chelating rod amphiphile (Fig. 1). The **VC** can carry out successive click reactions with an exceptional conversion efficiency owing to (i) stabilized catalytic Cu^{I} and reactants preserving the catalytic activity, and (ii) the reactive species in close proximity to the catalytic sites in the **VC** wall. Also, the self-encapsulation of the hydrophobic click products within the wall affects the

[a] *School of Materials Science and Engineering, Gwangju Institute of Science and Technology, 123 Cheomdangwagi-ro, Buk-gu, Gwangju 61005, Republic of Korea. E-mail: eunjilee@gist.ac.kr*
[b] *Graduate School of Analytical Science and Technology, Chungnam National University, 99 Daehak-ro, Yuseong-gu, Daejeon 34134, Republic of Korea*

† Electronic supplementary information (ESI) available. See DOI: 10.1039/c9qm00059c

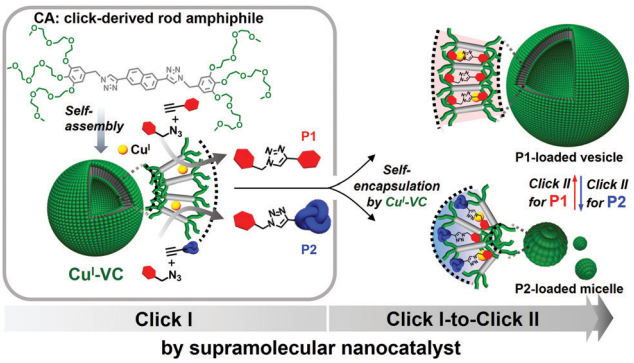

Fig. 1 Interfacial curvature-controllable supramolecular vesicular nanocatalyst (**VC**) for successive click I-to-click II reactions, formed by self-assembly of a click-derived rod amphiphile (**CA**) in water, depending on the molecular structure similarity of click reaction products **P1** and **P2** with the rod segment of **CA**. **P1** and **P2** are the click reaction products of benzyl azide with phenylacetylene or trimethylsilylacetylene, respectively.

interfacial curvature and thus the morphology of the **VC**, enabling the extensive use of **VC**s as smart nanomaterials.

Results and discussion

The click-derived rod amphiphile (**CA**) was synthesized by the CuAAC reaction of azide-terminated benzyl ether dendrons and diethynyl naphthalene (Fig. S1–S3, ESI†) and showed vesicular formation by aqueous self-assembly (Fig. 1 and Fig. S6b, ESI†). The Cu^{II}-chelation to the triazolyl moiety of **CA**, to provide the Cu^{I}-chelated **VC** (**Cu^{I}-VC**), was examined by ultraviolet-visible (UV-Vis), fluorescence, and ^{1}H nuclear magnetic resonance (NMR) spectroscopies (Fig. S6 and S7, ESI†). $CuSO_4$ (0.5 equiv. mol to **CA**) and sodium ascorbate (NaAsc, 3.0 equiv. mol to $CuSO_4$) were added to an aqueous solution of **CA** for the *in situ* reduction of Cu^{II} to Cu^{I} (Fig. 2). The stoichiometric ratio of **CA**:Cu^{II} was 2 : 1 (Fig. S6c, ESI†).[32] In the UV-Vis spectra, the characteristic d–d transition of Cu^{II} in the range 700–900 nm[33] disappeared, and new absorption peaks appeared at 600 and 750 nm after addition of $CuSO_4$ to the aqueous solution of **CA**, which could be assigned to a metal-to-ligand-transfer transition (Fig. S6d, ESI†).[34] The two peaks at 600 and 750 nm disappeared, and a band at 670 nm appeared after further reduction of Cu^{II} to Cu^{I} by NaAsc, indicating Cu^{I}-chelation by the triazolyl group of **CA**. The decrease in emission of **CA** after addition of $CuSO_4$, indicative of the Cu^{II}-chelation by the triazole group of **CA**, could be attributed to the reverse photoinduced electron transfer[35] involving electron donation from the excited naphthalene unit to the Cu^{II}-binding triazole group (Fig. S6e, ESI†).[36] The ^{1}H NMR signal of the triazole proton (H_c) of **CA** at 8.16 ppm measured in D_2O shifted upfield to 8.12 ppm upon addition of $CuSO_4$ (Fig. S7a, ESI†).[25] The H_g of **CA** shifted upfield by 0.06 ppm, suggesting the oxygen atoms next to the phenyl group were interacting with Cu^{II}. After further addition of NaAsc, the H_c- and H_g-signals showed a downfield shift of 0.04 and 0.03 ppm, respectively, indicating **CA**–Cu^{I} complex formation. Fig. S7b (ESI†) shows the plausible binding model of **CA**–Cu^{I}. The successful fabrication of vesicular structures of **CA**–Cu^{I} for **Cu^{I}-VC** was confirmed by transmission electron microscopy (TEM) (Fig. S8, ESI†). The unstained TEM images of both vesicular **CA**–Cu^{II} precatalyst and **CA**–Cu^{I} catalyst clearly showed the vesicular wall with enhanced contrast due to the chelation of Cu by the triazole group at the hydrophobic segment.

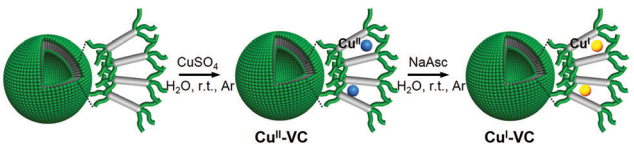

Fig. 2 Development of the **Cu^{I}-VC** for CuAAC.

The catalytic ability of **Cu^{I}-VC** was assessed by a ^{1}H NMR study. First, the CuAAC reaction using water-insoluble benzyl azide (5 mol equiv. to **CA** for **Cu^{I}-VC**) and phenylacetylene (5 equiv.) was performed for 24 h to generate click product **P1** in the presence of **Cu^{I}-VC** (Fig. S5a, ESI† and Table 1). After dissolving the resultant nanocatalyst in $CDCl_3$, a conversion efficiency of 99% was reached (Table 1, entry 1). The reaction did not occur in the absence of **Cu^{I}-VC** (entry 2). The enhanced reactivity of **Cu^{I}-VC** was confirmed by comparison to the reaction with Cu^{I}, showing moderate catalytic conversion of 31% (entry 3). This could be attributed to a closer contact of pre-organized hydrophobic reactants to stabilized catalytically active Cu^{I} sites confined in the walls of the supramolecular **Cu^{I}-VC**.[37]

Consequently, the water-insoluble click product **P1** was generated and self-encapsulated in the hydrophobic vesicular membrane. The ^{1}H NMR spectrum of **P1**-loaded **Cu^{I}-VC** in D_2O showed the upfield shift of naphthyl protons (H_d, H_e, and H_f, around 0.10–0.14 ppm), benzylic H_b (0.05 ppm), and triazolyl H_c (0.06 ppm) protons of **Cu^{I}-VC** compared with that of the original one in D_2O (Fig. S9c, ESI†). The upfield shifts of H_b, H_c,

Table 1 Comparison of **VC** catalyst efficiency in CuAAC[a]

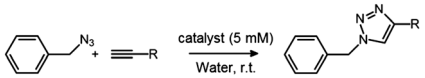

Entry	Catalyst	Alkyne	Time (h)	Conversion[b] (%)	Product name
1	**Cu^{I}-VC**	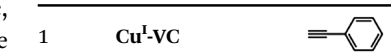	24	99	**P1**
2	·		24	0	·
3	Cu^{I}[c]		24	31	**P1**
4	**Cu^{I}-VC**	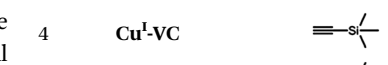	24	98	**P2**
5	·		24	0	·
6	**P2**-loaded **Cu^{I}-VC**		24	99	**P1**
7	**P1**-loaded **Cu^{I}-VC**		24	36	**P2**

[a] All reactions were carried out with 5 equiv. mol (12.5 μmol) of benzyl azide and alkyne in 0.5 mL distilled water at room temperature. [b] Reaction conversion was determined by ^{1}H NMR spectroscopy. [c] Cu^{I} was prepared by addition of 3.0 equiv. NaAsc into the 0.1 mM $CuSO_4$ solution under Ar atmosphere.

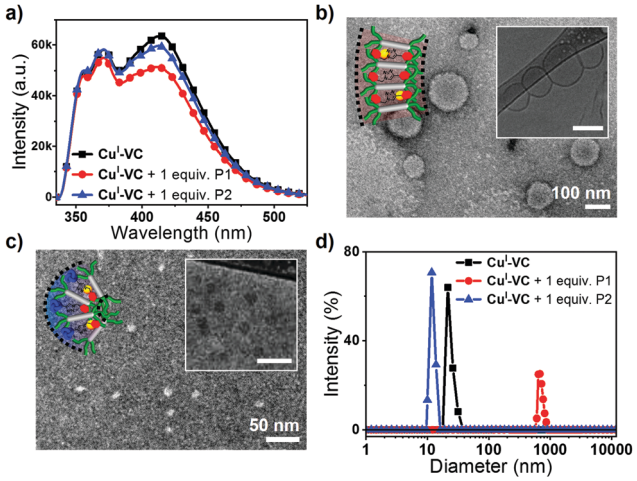

Fig. 3 (a) Emission spectra (λ_{ex} = 260 nm) of **Cu^{I}-VC**, **P1**-, and **P2**-loaded **Cu^{I}-VC** in water. Negatively stained TEM image of (b) **P1**- and (c) **P2**-loaded **Cu^{I}-VC** (0.02 mM) with 2 wt% uranyl acetate. Insets of (b and c) show the cryo-TEM image. Inset scale bar equals (b) 100 and (c) 50 nm, respectively. (d) Hydrodynamic diameters of **Cu^{I}-VC**, **P1**-, and **P2**-loaded **Cu^{I}-VC**.

H_d, H_e, and H_f could be ascribed to the shield effect of **P1** by the π–π stacking with the rod amphiphile **CA**.[38] The absorbance of **Cu^{I}-VC** decreased and the emission was quenched after generation of **P1** by the CuAAC reaction (Fig. S10, ESI† and Fig. 3a) which could be attributed to the energy transfer of **Cu^{I}-VC** to **P1** due to the π–π stacking between the aromatic block of **CA** and **P1**.[39] TEM images revealed that the vesicular structure of **Cu^{I}-VC** remains intact after loading **P1** by the CuAAC reaction (Fig. 3b). Even in the presence of excess reactants, precipitating **P1** (white solid) by the constant reactivity of **Cu^{I}-VC**, the vesicular structure was maintained without rupture (Fig. S11a and b, ESI†).

To confirm the catalytic activity of **Cu^{I}-VC**, **P2** with a bulky trimethyl group was synthesized using the CuAAC reaction of trimethylsilylacetylene and benzyl azide (Fig. 1, Table 1 and Fig. S5b, ESI†). **Cu^{I}-VC** shows an excellent conversion efficiency of 98% (entry 4). When the **P2**-forming CuAAC reaction was carried out without **Cu^{I}-VC**, the reaction did not occur as expected (entry 5). The ^{1}H NMR spectrum of **Cu^{I}-VC** with **P2** measured in D_2O showed an upfield shift similar to that observed for **P1**-loaded **Cu^{I}-VC** in D_2O, indicating the encapsulation of **P2** by **Cu^{I}-VC** (Fig. S12c, ESI†). The **P2**-loaded **Cu^{I}-VC** showed the formation of micelles of diameter ∼10 nm (Fig. 3c and Fig. S13c, ESI†), which is twice the molecular length of fully extended **CA** (Fig. S6a, ESI†). The emission quenching of **Cu^{I}-VC** upon generation of **P2** suggests the intercalation of **P2** within the hydrophobic wall of **Cu^{I}-VC** (Fig. 3a). The smaller decrease in the emission of **P2**-loaded **Cu^{I}-VC** than that of **P1**-loaded **Cu^{I}-VC** could be the result of less effective π–π stacking of **P2** with the hydrophobic rod segments of the **CA** nanocatalyst.[40] The bulky trimethyl groups of **P2** may hinder the close packing of **CA** within the membrane of **Cu^{I}-VC**, resulting in morphological transformation of **Cu^{I}-VC** from vesicle to micelle. Dynamic light scattering (DLS) revealed an increase in the average hydrodynamic diameter (R_H) of **P1**-intercalated **Cu^{I}-VC** (from ∼21 nm to ∼600 nm) (Fig. 3d). A decrease in the R_H of **P2**-intercalated **Cu^{I}-VC** was observed (from ∼21 nm to ∼10 nm) compared with **Cu^{I}-VC**. Therefore, the molecular structure similarity of the click reaction products with the hydrophobic rod segment of **CA** may affect the interfacial curvature of supramolecular nanocatalyst **Cu^{I}-VC**, resulting in a morphological change. For instance, the high structural compatibility of **P1** with **CA** could enable the effective encapsulation of **P1** within the membrane of **Cu^{I}-VC**. The π–π stacking of **P1** with **CA** could be optimized as **P1** and the rigid hydrophobic segment of **CA** are arranged in parallel, which decreased the interfacial curvature of the wall, leading to an increase in **Cu^{I}-VC** size.[41] These results are consistent with the entropic cost of intercalating molecules with increased volume, which is responsible for the vesicle-to-micelle morphological change.[42]

As the interfacial curvature of **Cu^{I}-VC** can be tuned by the molecular architecture of click products, we studied whether the reversible morphological transformation of nanocatalyst from micellar aggregates to vesicles could be achieved by sequential click reactions to form **P1** using **P2**-loaded **Cu^{I}-VC** (Fig. 4a). The CuAAC reaction of benzyl azide and phenylacetylene catalyzed by **P2**-loaded **Cu^{I}-VC** was performed (Table 1, entry 6). The catalytic activity of the **P2**-loaded nanoreactor still shows a tremendous conversion efficiency of 99% despite the pre-loading of **P2** in **Cu^{I}-VC**. In the ^{1}H NMR spectrum of **P2**-loaded **Cu^{I}-VC** after the CuAAC reaction to form **P1** in D_2O, H_b, H_c, H_d, H_e, and H_f are significantly downfield shifted (0.05–0.09 ppm), probably indicating a strong hydrogen bonding interaction between the triazolyl and naphthyl protons of **CA** and the aromatic protons and nitrogen atoms in the triazole moiety of **P1** and **P2** (Fig. 4b).[38] H_a and H_g showed a moderate downfield shift (0.05 ppm), which suggests the enhanced hydrogen bonding interaction of polyethylene oxide chains of **CA** with water. However, after dissolving the resultant nanocatalyst in $CDCl_3$, only **P1** signals were detected in the ^{1}H NMR spectrum (Fig. 4b and Fig. S14, ESI†). Fluorescence quenching of **P2**-loaded **Cu^{I}-VC** was observed after the **P1**-forming CuAAC reaction (Fig. S15b, ESI†). The TEM experiment showed the presence of vesicles (Fig. 4c). These results can be explained by preloaded **P2** in **Cu^{I}-VC** being replaced with **P1** and released into the aqueous solution because **P1** has greater molecular structure compatibility with **CA**, which can form a more stable vesicle through π-stacking. The released **P2** to the aqueous phase was confirmed by ^{1}H NMR experiment. The transformation of **P2**-loaded nanocatalyst to a vesicular structure by successive click reactions was further confirmed using hydrophilic dye fluorescein isothiocyanate (FITC) that can be encapsulated in the interior cavity of the vesicle (Fig. S16a, ESI†).[43] As expected, the fluorescence micrograph clearly showed bright green-emitting spherical aggregates, indicating the formation of a vesicle (Fig. 4d and Fig. S16b, ESI†).

The morphological transformation of **P1**-loaded nanocatalyst was also demonstrated by conducting **P2**-forming CuAAC reaction (Fig. 5, Fig. S14 and S17, ESI†). The **P1**-loaded vesicular nanocatalyst encapsulating FITC in inner aqueous compartment could release the FITC fluorescent dyes into the outer aqueous phase after performing a **P2**-forming CuAAC reaction as a result

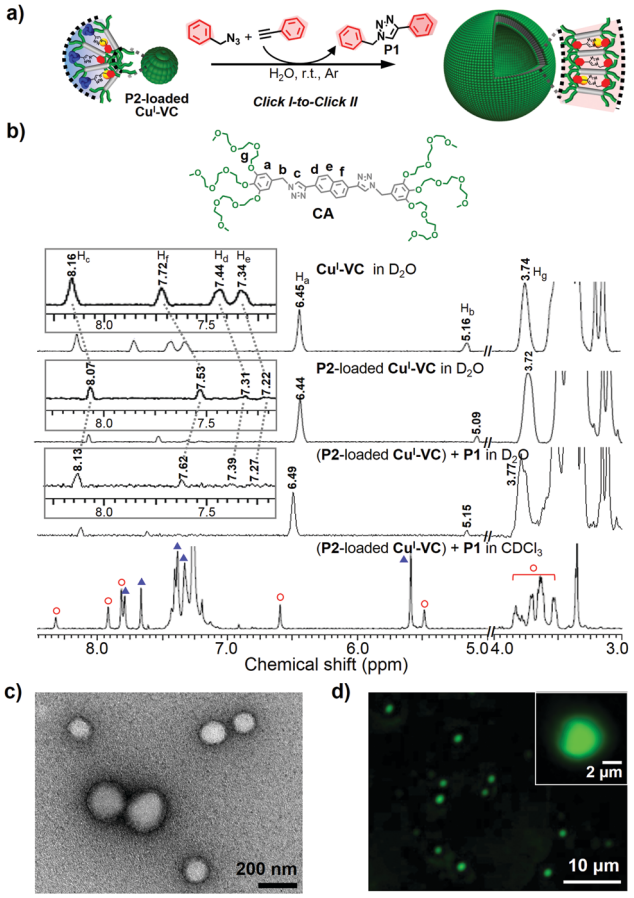

Fig. 4 (a) Successive click reactions of nanocatalyst, resulting in the morphological change of **Cu^{I}-VC** from micelle to vesicle. (b) ^{1}H NMR spectra of **Cu^{I}-VC** and **P2**-loaded **Cu^{I}-VC** measured in D_2O and **P2**-loaded **Cu^{I}-VC** after click reaction to generate **P1** measured in D_2O and $CDCl_3$. Red hollow circle (○) and blue triangle (▲) denote **CA** and **P1**, respectively. More detailed information is in the ESI.† (c) Negatively stained TEM image and (d) fluorescence micrograph of the **P2**-loaded **Cu^{I}-VC** after click reaction to synthesize **P1**. Inset of (d) shows the vesicle containing FITC within the inner aqueous medium separated by a wall from the outer aqueous solution. Green fluorescence: FITC.

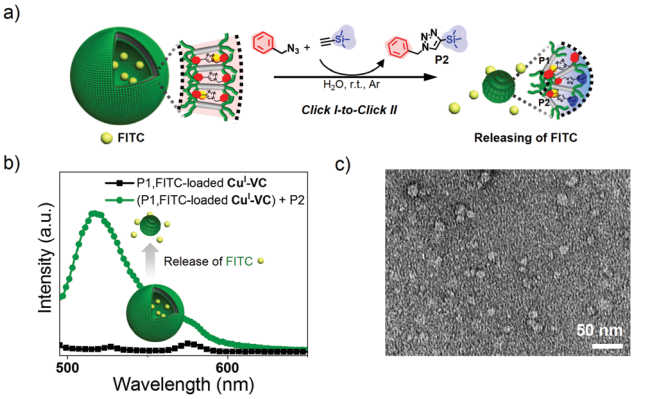

Fig. 5 (a) Morphological transformation of **Cu^{I}-VC** from vesicle to micelle by successive click reactions of nanocatalyst, leading to controllable loading/release of FITC payloads. (b) Emission enhancement of the FITC-released aqueous solution of **P1**-loaded **Cu^{I}-VC** (0.5 mM) incorporating FITC after click reaction to form **P2**. (c) Negatively stained TEM image of **P1**-loaded **Cu^{I}-VC** after **P2**-forming CuAAC reaction with 2 wt% uranyl acetate.

of the nanostructural transformation to micelle (Fig. 5b). The TEM image clearly showed the micellar structures with a diameter of ~10 nm (Fig. 5c). The ^{1}H NMR spectrum of the resultant micelles dissolved in $CDCl_3$ indicated the presence of both **P1** and **P2** within the micelle core (Fig. S14, ESI†) which could be because the preloaded **P1** is not fully replaced with **P2** due to the higher structural compatibility of **P1** with **CA**. The conversion efficiency of **P2** production using **P1**-loaded **Cu^{I}-VC** was calculated to be relatively low (36%) (Table 1, entry 7). This result could be attributed to the strong mutual interaction between **CA** and **P1**, limiting the access of trimethylsilylacetylene and benzyl azide to the catalytic Cu^{I} located in the vesicular wall. Therefore, the molecular packing constraint induced by preloaded products within the hydrophobic wall of the nanocatalyst should be considered for performing successive click reactions.

The recyclable catalytic activity of **Cu^{I}-VC** with structural transformable capability was further confirmed by conducting a visually detectable click reaction *via* a fluorescent color change of a **Cu^{I}-VC** solution. The conversion of water-insoluble nonfluorescent reactants to fluorescent products by the CuAAC reaction can help detect the click reaction using the naked eye. The hydrophobic coumarin derivatives were utilized as a target click product. Upon adding coumarin into aqueous **Cu^{I}-VC** solution, characteristic absorption of coumarin (~280 nm) appeared while the fluorescence of **Cu^{I}-VC** was quenched, indicating the presence of coumarin within the hydrophobic segment of **Cu^{I}-VC** (Fig. S18, ESI†). To generate a coumarin-based fluorescent click product with different structural similarities to **CA**, we synthesized 3-azido-7-hydroxycoumarin, a nonfluorescent azide (Fig. S4, ESI†).[44,45] The fluorescent emission of the coumarin moiety in 3-azido-7-hydroxycoumarin is quenched by the lone pair of electrons from the azido group.[46,47] Phenylacetylene and trimethylsilylacetylene were also used for the CuAAC reactions with 3-azido-7-hydroxycoumarin (Fig. 6a). The resulting click products of phenylacetylene and trimethylsilylacetylene with 3-azido-7-hydroxycoumarin were referred to as **CP1** and **CP2**, respectively (Fig. 6a). As expected, the blue color of 5 mM **Cu^{I}-VC** solution became turquoise under irradiation at 365 nm, indicating the formation of **CP1** and the subsequent loading within the **Cu^{I}-VC** vesicular membrane. In contrast, the **CP2**-containing **Cu^{I}-VC** solution showed relatively weak green emission under UV irradiation. A new absorption band around 340 nm appeared for both **CP1**- and **CP2**-loaded **Cu^{I}-VC** (Fig. 6b), and the fluorescence of **Cu^{I}-VC** was quenched (Fig. 6c). These results indicate that click products **CP1** and **CP2** were incorporated within the **Cu^{I}-VC** wall. Notably, a characteristic emission peak of **CP1** at 480 nm appeared for **CP1**-loaded **Cu^{I}-VC** when excited at the wavelength of 260 nm which indicates the fluorescence resonance energy transfer (FRET) due to the close proximity of **CP1** and the rod block of **CA**.[48] The electron lone pair of the azido moiety of 3-azido-7-hydroxycoumarin could be localized as the triazole ring is formed in **CP1**, leading to the activation of

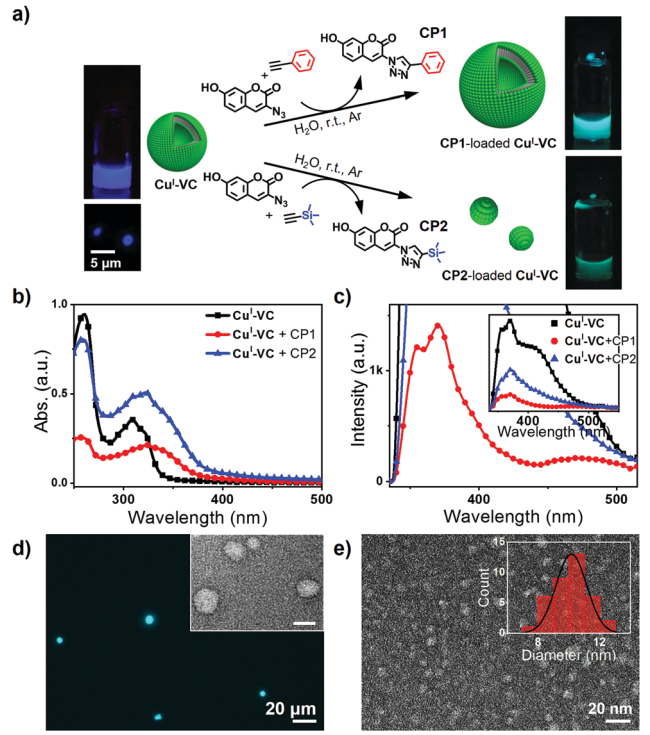

Fig. 6 (a) **Cu^{I}-VC** nanocatalyst with images of a 5 mM **Cu^{I}-VC** solution under UV irradiation (λ_{ex} = 365 nm). Change in (b) absorption and (c) emission spectra of 0.02 mM **Cu^{I}-VC** upon CuAAC reaction to generate **CP1** and **CP2**, respectively (λ_{ex} = 260 nm). (d) Fluorescence micrograph of **CP1**-loaded **Cu^{I}-VC**. Inset shows the negatively stained TEM image of **CP1**-loaded **Cu^{I}-VC** with a scale bar of 50 nm. (e) Negatively stained TEM image of **CP2**-incorporated **Cu^{I}-VC**. Inset shows the diameter distribution of the micelle.

fluorescence.[46,47] The emergence of the FRET signal demonstrated efficient stacking between **CP1** and the rod amphiphile **CA**. The fluorescence micrograph of the **CP1**-loaded **Cu^{I}-VC** confirmed the presence of spherical structures (Fig. 6d), and TEM revealed the intact vesicular structure of **CP1**-encapsulated **Cu^{I}-VC** (inset of Fig. 6d and Fig. S19, ESI†). Loading of **CP2** with an unsymmetric structure imposed by the bulky trimethyl group into **Cu^{I}-VC** showed the formation of the micellar aggregates (Fig. 6e). These results are consistent with the morphological transition from vesicles to micelles observed for **Cu^{I}-VC** when synthesizing **P1** and **P2** based on the benzyl azide.

Conclusions

In summary, we have developed an aqueous supramolecular nanocatalyst based on the self-assembly of the click-derived rod amphiphile, capable of successive click reactions, which maintained excellent catalytic efficiency. The self-transformable behavior of the nanocatalyst was controlled by encapsulating structurally compatible hydrophobic click reaction products with a rod amphiphile, which, in turn, affects the interfacial curvature of the nanocatalyst. The morphological transformability enables the click nanoreactor/catalyst potential for *in situ* production of on demand payloads and controllable loading/release of such payloads, including drugs, imaging agents, and chemical species. This can further broaden the potential applications of supramolecular nanocatalysts into the field of smart nanobiomedicine and chemo/biosensors.

Conflicts of interest

There are no conflicts of interest to declare.

Acknowledgements

This research was supported by Basic Science Research Program (2016R1A2B4012322) through the National Research Foundation of Korea (NRF). We thank Prof. B. K. Cho for the discussion of amphiphile **CA** synthesis.

References

1 P. Tanner, P. Baumann, R. Enea, O. Onaca, C. Palivan and W. Meier, *Acc. Chem. Res.*, 2011, **44**, 1039–1049.
2 C. LoPresti, H. Lomas, M. Massignani, T. Smart and G. Battaglia, *J. Mater. Chem.*, 2009, **19**, 3576–3590.
3 D. E. Discher and A. Eisenberg, *Science*, 2002, **297**, 967–973.
4 T. Rispens and J. B. F. N. Engberts, *Org. Lett.*, 2001, **3**, 941–943.
5 G. Hamasaka, T. Muto and Y. Uozumi, *Angew. Chem., Int. Ed.*, 2011, **50**, 4876–4878.
6 M. Liu, X. Zhu, L. Wu, X. Zhou, J. Li and J. Ma, *RSC Adv.*, 2015, **5**, 38264–38270.
7 R. J. R. W. Peters, I. Louzao and J. C. M. van Hest, *Chem. Sci.*, 2012, **3**, 335–342.
8 D. M. Vriezema, P. M. L. Garcia, N. S. Oltra, N. S. Hatzakis, S. M. Kuiper, R. J. M. Nolte, A. E. Rowan and J. C. M. van Hest, *Angew. Chem., Int. Ed.*, 2007, **46**, 7378–7382.
9 O. Rifaie-Graham, S. Ulrich, N. F. B. Galensowske, S. Balog, M. Chami, D. Rentsch, J. R. Hemmer, J. R. de Alaniz, L. F. Boesel and N. Bruns, *J. Am. Chem. Soc.*, 2018, **140**, 8027–8036.
10 D. M. Vriezema, M. C. Aragonès, J. A. A. W. Elemans, J. J. L. M. Cornelissen, A. E. Rowan and R. J. M. Nolte, *Chem. Rev.*, 2005, **105**, 1445–1489.
11 M. A. C. Stuart, W. T. S. Huck, J. Genzer, M. Müller, C. Ober, M. Stamm, G. B. Sukhorukov, I. Szleifer, V. V. Tsukruk, M. Urban, F. Winnik, S. Zauscher, I. Luzinov and S. Minko, *Nat. Mater.*, 2010, **9**, 101–113.
12 C. G. Palivan, R. Goers, A. Najer, X. Zhang, A. Car and W. Meier, *Chem. Soc. Rev.*, 2016, **45**, 377–411.
13 L. Jiang, X. Huang, D. Chen, H. Yan, X. Li and X. Du, *Angew. Chem., Int. Ed.*, 2017, **56**, 2655–2659.
14 W. Zhang and C. Gao, *J. Mater. Chem. A*, 2017, **5**, 16059–16104.
15 Z.-Q. Cao, Y.-C. Wang, A.-H. Zou, G. London, Q. Zhang, C. Gao and D.-H. Qu, *Chem. Commun.*, 2017, **53**, 8683–8686.
16 M.-H. Li and P. Keller, *Soft Matter*, 2009, **5**, 927–937.

17 S. Mura, J. Nicolas and P. Couvreur, *Nat. Mater.*, 2013, **12**, 991–1003.
18 H. C. Kolb, M. G. Finn and K. B. Sharpless, *Angew. Chem., Int. Ed.*, 2001, **40**, 2004–2021.
19 V. V. Rostovtsev, L. G. Green, V. V. Fokin and K. B. Sharpless, *Angew. Chem., Int. Ed.*, 2002, **41**, 2596–2599.
20 J.-F. Lutz and Z. Zarafshani, *Adv. Drug Delivery Rev.*, 2008, **60**, 958–970.
21 D. S. Tyler, J. Vappiani, T. Cañeque, E. Y. N. Lam, A. Ward, O. Gilan, Y.-C. Chan, A. Hienzsch, A. Rutkowska, T. Werner, A. J. Wagner, D. Lugo, R. Gregory, C. R. Molina, N. Garton, C. R. Wellaway, S. Jackson, L. MacPherson, M. Figueiredo, S. Stolzenburg, C. C. Bell, C. House, S.-J. Dawson, E. D. Hawkins, G. Drewes, R. K. Prinjha, R. Rodriguez, P. Grandi and M. A. Dawson, *Science*, 2017, **356**, 1397–1401.
22 J.-F. Lutz, *Angew. Chem., Int. Ed.*, 2008, **47**, 2182–2184.
23 C. J. Hawker and K. L. Wooley, *Science*, 2005, **309**, 1200–1205.
24 H. C. Kolb and K. B. Sharpless, *Drug Discovery Today*, 2003, **8**, 1128–1137.
25 C. Deraedt, N. Pinaud and D. Astruc, *J. Am. Chem. Soc.*, 2014, **136**, 12092–12098.
26 H. Struthers, T. L. Mindt and R. Schibli, *Dalton Trans.*, 2010, **39**, 675–696.
27 B. Schulze and U. S. Schubert, *Chem. Soc. Rev.*, 2014, **43**, 2522–2571.
28 Y. H. Lau, P. J. Rutledge, M. Watkinson and M. H. Todd, *Chem. Soc. Rev.*, 2011, **40**, 2848–2866.
29 J. E. Moses and A. D. Moorhouse, *Chem. Soc. Rev.*, 2007, **36**, 1249–1262.
30 A. Maisonial, P. Serafin, M. Traïkia, E. Debiton, V. Théry, D. J. Aitken, P. Lemoine, B. Viossat and A. Gautier, *Eur. J. Inorg. Chem.*, 2008, 298–305.
31 M. R. Jones, E. Mathieu, C. Dyrager, S. Faissner, Z. Vaillancourt, K. J. Korshavn, M. H. Lim, A. Ramamoorthy, V. W. Yong, S. Tsutsui, P. K. Stys and T. Storr, *Chem. Sci.*, 2017, **8**, 5636–5643.
32 I. Kim, N.-E. Lee, Y.-J. Jeong, Y.-H. Chung, B.-K. Cho and E. Lee, *Chem. Commun.*, 2014, **50**, 14006–14009.
33 H. Irie, K. Kamiya, T. Shibanuma, S. Miura, D. A. Tryk, T. Yokoyama and K. Hashimoto, *J. Phys. Chem. C*, 2009, **113**, 10761–10766.
34 T. J. Meyer, *Pure Appl. Chem.*, 1986, **58**, 1193–1206.
35 A. P. de Silva, T. S. Moody and G. D. Wright, *Analyst*, 2009, **134**, 2385–2393.
36 Y.-C. Hsieh, J.-L. Chir, H.-H. Wu, P.-S. Chang and A.-T. Wu, *Carbohydr. Res.*, 2009, **344**, 2236–2239.
37 L. Qin, L. Zhang, Q. Jin, J. Zhang, B. Han and M. Liu, *Angew. Chem., Int. Ed.*, 2013, **52**, 7761–7765.
38 Y. Zhao, Y. Li, Y. Li, C. Huang, H. Liu, S.-W. Lai, C.-M. Che and D. Zhu, *Org. Biomol. Chem.*, 2010, **8**, 3923–3927.
39 V. K. Praveen, C. Ranjith, E. Bandini, A. Ajayaghosh and N. Armaroli, *Chem. Soc. Rev.*, 2014, **43**, 4222–4242.
40 N. K. Allampally, A. Florian, M. J. Mayoral, C. Rest, V. Stepanenko and G. Fernández, *Chem. – Eur. J.*, 2014, **20**, 10669–10678.
41 Y. Mai and A. Eisenberg, *Chem. Soc. Rev.*, 2012, **41**, 5969–5985.
42 R. J. Hickey, J. Koski, X. Meng, R. A. Riggleman, P. Zhang and S.-J. Park, *ACS Nano*, 2014, **8**, 495–502.
43 M. R. Molla, P. Rangadurai, L. Antony, S. Swaminathan, J. J. de Pablo and S. Thayumanavan, *Nat. Chem.*, 2018, **10**, 659–666.
44 C. Wang, L. Lu, W. Ye, O. Zheng, B. Qiu, Z. Lin, L. Guo and G. Chen, *Analyst*, 2014, **139**, 656–659.
45 K. Sivakumar, F. Xie, B. M. Cash, S. Long, H. N. Barnhill and Q. Wang, *Org. Lett.*, 2004, **6**, 4603–4606.
46 Y. Liu, T. Pauloehrl, S. I. Presolski, L. Albertazzi, A. R. A. Palmans and E. W. Meijer, *J. Am. Chem. Soc.*, 2015, **137**, 13096–13105.
47 C. Besanceney-Webler, H. Jiang, T. Zheng, L. Feng, D. S. del Amo, W. Wang, L. M. Klivansky, F. L. Marlow, Y. Liu and P. Wu, *Angew. Chem., Int. Ed.*, 2011, **50**, 8051–8056.
48 M. M. Hanczyc, S. M. Fujikawa and J. W. Szostak, *Science*, 2003, **302**, 618–622.